

pubs.acs.org/jced Article

Cation Dependence of Gas Adsorption in Clinoptilolite and RHO Zeolites Using Monte Carlo Simulation: A Linear Model

Micah L. Welsch and Brian B. Laird*



Cite This: J. Chem. Eng. Data 2024, 69, 2031–2040



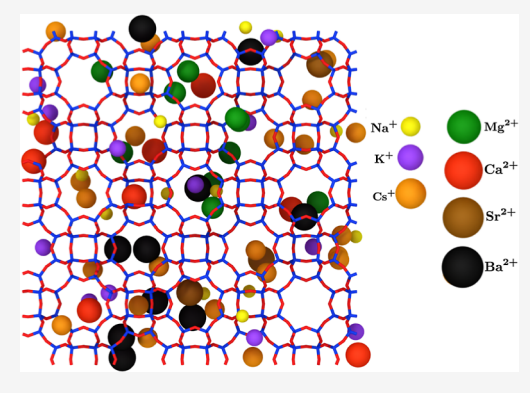
ACCESS I

Metrics & More

Article Recommendations

Supporting Information

ABSTRACT: Zeolites have tremendous potential as adsorbents for the selective separation and storage of gases in many industrial processes. The extent and selectivity of gas adsorption are dependent on a number of zeolite properties, such as pore diameter, accessible volume, and silicon-to-aluminum ratio. In addition, the existence of aluminum in the framework requires the presence of cations to maintain charge neutrality, and the identity of these extra-framework cations will also have a significant effect on adsorption. In this work, the continuous fractional component Monte Carlo method was used to examine the effect of the size and the charge of these cations on the adsorption of a variety of gases (CH_4, N_2, ACO_2) in two representative zeolite frameworks, clinoptilolite (heulandite) (CLI) and RHO at 298.15 K, using a range of pressures from 0.1 to 60 bar for a variety of mono- and divalent cations $(Na^+, K^+, Cs^+, Mg^{2+}, Ca^{2+}, Sr^{2+}, ACO_2)$ and ACO_2 in the single-cation systems revealed unique



trends in the size and charge for each gas. To examine the combined effect of multiple cation types, adsorption was calculated at 0.5 and 30 bar in several two-cation systems, in which the effects of the size and charge were isolated and examined. The resulting adsorption varied linearly with the mole fraction of each two-cation mixture. A linear model is proposed to describe the loading of gases in CLI and RHO zeolites containing complex cation mixtures. Loading predicted by this model showed excellent agreement with direct simulation of gas adsorption in randomized seven-cation systems, suggesting that the adsorption effect of each cation is additive among the zeolite frameworks tested.

1. INTRODUCTION

For many industrial processes, improvements to the selective separation and storage of gases can yield significant advantages. For example, the separation of CO_2 from air $(N_2 \text{ and } O_2)$ or natural gas (CH₄) has been of long running interest in the energy industry. Another example is the Haber–Bosch process⁴ in which ammonia must be separated from unreacted nitrogen and hydrogen gas. This is typically done through condensation of the product ammonia from the reactant gases; however, this process can be costly to set up and operate. Gas separation and storage through adsorption can serve as a cheaper alternative to current separation methods provided an appropriate sorbent exists. Common low-cost materials include amines and meso- and microporous materials. One such class of microporous materials are metal organic frameworks (MOFs),5,6 which provide many strong candidates for gas storage and separation. Currently, the viability of MOF synthesis at an industrial scale is not ideal,⁷ and cost reduction must be assessed on a case-by-case basis.

Of significant promise are zeolites, a class of microporous aluminosilicate materials, which are appreciably less expensive than MOFs while maintaining high gas selectivity in separations. There are more than 250 zeolite frameworks, both synthetic and naturally occurring, and much like MOFs, the properties of these frameworks are tunable, substantially increasing the

number of possible distinct materials. Extensive work has been done to characterize and quantify the separation performance of different zeolites both experimentally $^{9-12}$ and computationally. 13,14

The separation performance of zeolites can be optimized through the variation of the framework type and extra-framework cation density, the latter resulting from valency, position, and silicon-to-aluminum ratio (the ratio of framework silicon to aluminum atoms, Si/Al), all of which have been shown to influence gas adsorption. One way to characterize these properties is to systematically compare gas adsorption in frameworks exchanged with cations of varying sizes and charge. One conclusion of previous experimental and computational studies is that there is a direct relationship between gas adsorption and cation size at constant valency. Lozinska et al. Teported such a trend with CO₂ adsorption in zeolite RHO showing higher adsorption in Li⁺ exchanged systems over larger

Received: December 8, 2023 Revised: February 9, 2024 Accepted: February 14, 2024 Published: March 6, 2024





alkali metals. Monte Carlo (MC) studies report a similar relationship in the adsorption of alkanes in MFI¹⁹ and N₂ in Faujasite (FAU).²¹

When considering cation mobility, it was found by Lozinska et al. that Na+ was more readily displaced than Cs+, leading to a larger than expected increase in CO₂ adsorption for the Na⁺exchanged framework. Adsorption of N₂, an adsorbate with a larger kinetic diameter and weaker quadrupole moment, 22 showed near-zero adsorption due to an inability to displace Na⁺ or Cs⁺ demonstrating the importance of adsorbate-cation interactions. Another property that impacts gas adsorption is the framework flexibility. The RHO framework, for example, has been shown to undergo a structural transformation upon dehydration and cation exchange transitioning from the centrosymmetric $Im\overline{3}m$ space group to the noncentrosymmetric I-43m. 17 At CO₂ pressures of 2 bar and above, the structure has been seen to revert back to its original centrosymmetric form increasing the adsorption capacity. ²³ In the current study, only the centrosymmetric Im3m RHO framework is considered and treated as rigid in order to probe the effect that extra-framework cation size and charge, independent of framework flexibility, have on gas adsorption.

Adsorbate—cation interactions have also been shown to play a significant role alongside steric effects in an MC study published by Dangi et al.²⁰ CO₂ was shown to adsorb based on the cation size in a Linde-type L (LTL) zeolite when charge balanced with alkali metal cations with the highest adsorption again observed in the Li⁺ system. Systems containing alkaline earth metal cations did not exhibit the same size trend due to the differences in charge interactions. Partial cation exchange into frameworks with preexisting cation mixtures has also been studied experimentally in systems such as clinoptilolite (CLI), a heulandite (HEU)-type framework that naturally contains Na⁺, K⁺, Ca²⁺, and Mg²⁺. Kennedy et al.²² measured gas adsorption in CLI samples partially exchanged with alkali, alkaline earth, and transition metal cations. The same trend between cation size and adsorption was observed for CO2 in samples exchanged with alkali metals, with Li⁺ yet again yielding the highest loading.

Such systematic studies of the effect of cation identity on gas adsorption have primarily focused on single-cation systems; however, naturally occurring zeolites generally contain a complex mixture of extra-framework cations. As a result, although there is a good understanding of the effect of cation identity in single-cation zeolites on adsorption, such an understanding for multication zeolites is lacking. In this work, MC simulation is used to examine the adsorption of a variety of gases (CH₄, N₂, and CO₂) into CLI and RHO zeolites at a fixed Si/Al ratio using a variety of monovalent (Na⁺, K⁺, and Cs⁺) and divalent (Mg²⁺, Ca²⁺, Sr²⁺, and Ba²⁺) extra-framework cations. Adsorption was calculated in single-cation systems as well as in select two-cation combinations. Over most of the gas pressure range, two-cation adsorption was found to be well approximated as linear in the cation mole fractions. Motivated by this result, we propose a linear model for the adsorption of gases in zeolites with which the loading for an arbitrary multication-type mixture can be predicted based entirely on the single-cation adsorption

The structure of the article is as follows: The details of the system setup and subsequent simulations are discussed in Section 2. In Section 3, the results for the adsorption of selected gases are presented for both single and two cation-type zeolites. A linear predictive model for the adsorption of gases is presented

and tested in Section 4 and in Section 5 we summarize and conclude.

2. SIMULATION DETAILS

The simulation of gas adsorption into the CLI and RHO frameworks was carried out using the continuous fractional

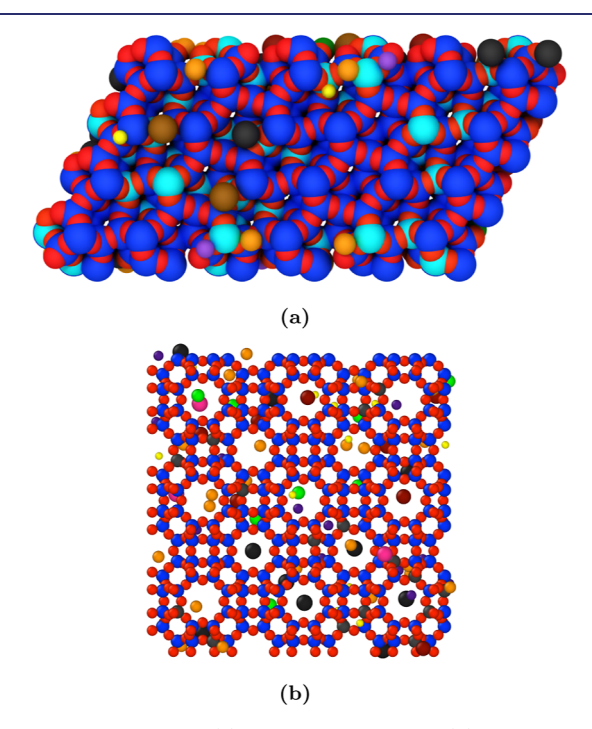


Figure 1. $3 \times 3 \times 4$ CLI (a) and $3 \times 3 \times 3$ RHO (b) supercells with random aluminum distributions and cation compositions.

component Monte Carlo (CFCMC)²⁴ routine within the RASPA²⁵ package over a pressure range of 0.1-60 bar at 298.15 K. The CFCMC ensemble was chosen over the standard grand canonical ensemble for its ability to treat inserted molecules as fractional, a task that is accomplished by incorporating a coupling parameter, λ , into the MC move-set that varies continuously from zero to one. This generally improves the efficiency of particle insertions into dense systems, as molecules are initially inserted with no interactions ($\lambda = 0$) and are eventually fully turned on $(\lambda = 1)$ based on the same acceptance rules as other MC moves. MC moves consisting of translations, rotations, and reinsertions were used to sample gas occupancy within each zeolite. For the cations, a combination of standard translational and large translational moves was applied. The maximum displacement for standard translational moves was dynamically optimized to achieve an acceptance ratio of 50%, while the larger translational moves allowed for jumps to anywhere within the system to enhance ergodicity. The latter move type is important to consider for systems where some aluminum sites are unoccupied (i.e., two-cation systems).

In this study, idealized structures for CLI and RHO were utilized with unit cell parameters taken from the International Zeolite Association database. 26 Real zeolites deviate from these idealized structures with varying levels of defects that affect the precise magnitudes of gas adsorption; however, a detailed study of such effects is beyond the scope of this work, which is focused on understanding generic aspects of gas adsorption in zeolites and not on precise predictions of specific systems. The CLI unit cell is a monoclinic HEU-type structure with a = 17.5230 Å, b =

Table 1. Chemical Compounds and Models

chemical name	chemical formula	CAS no	model
CLI-4.6A	$[(SiO_2)(AlO_2)_x]M_{x/n}$	1318-02-1	Dangi et al. ²⁰
RHO-10.8A	$[(SiO_2)(AlO_2)_x]M_{x/n}$	1318-02-1	Dangi et al. ²⁰
methane	CH_4	74-82-8	TraPPE-UA (Zeo) ³⁰
nitrogen	N_2	7727-37-9	TraPPE-EH ³⁵
carbon dioxide	CO_2	12-38-9	three-site ³⁶

Table 2. Self-Interaction Parameters and Charges for Cation, Adsorbate, and Adsorbent Atom Types

atom type	σ (Å)	ε (K)	q (e)
Si	0.0	0.0	2.4
Al	0.0	0.0	1.7
O_{zeo}	3.04	168.07	-1.2
Na ⁺	1.746	50.34	0.7
K ⁺	2.29	45.04	0.7
Cs ⁺	2.724	7.07	0.7
Mg^{2+}	3.022	55.8	1.4
Ca ²⁺	3.4	119.64	1.4
Sr ²⁺	3.642	118.19	1.4
Ba ²⁺	3.704	183.09	1.4
CH_4	3.72	158.5	0.0
N_{N_2-N}	3.318	36.43	-0.4048
N_{N_2-com}	0.0	0.0	0.8096
C_{CO_2}	3.830	46.65	0.6512
O_{CO_2}	3.360	76.44	-0.3256

Table 3. Critical Parameters and Acentric Factors of Gases Simulated in This Study³⁸

atom type	$T_{c}(K)$	$P_{\rm c}$ (bar)	ω
CH_4	190.56	45.99	0.0114
N_2	126.19	33.95	0.0372
CO_2	304.13	73.77	0.2239

17.6440 Å, and c = 7.410 Å lattice parameters and a C12/m1 space group. The RHO unit cell is a cubic structure with a lattice parameter of 14.9190 Å and an $Im\overline{3}m$ space group. The zeolites examined were held rigid throughout the simulations. $3 \times 3 \times 4$ and $3 \times 3 \times 3$ supercells were constructed (Figure 1) to satisfy 10 and 12 Å cutoffs for the van der Waals (vdW) and Coulombic energy interactions, respectively. All simulations utilized three-dimensional periodic boundary conditions. Crystallographic Information Framework (.cif) files for the zeolite structures used in these simulations are given in the Supporting Information.

Due to the difficulty in measuring aluminum distributions within zeolites²⁸ and the determination of such a quantity being outside the scope of this work, the Si/Al ratios for CLI and RHO were generated by random placement of aluminum within a silica starting structure. No Al-O-Al connections were allowed within the frameworks in accordance with the Löwenstein rule, a common aluminosilicate convention with some exceptions.²⁹ Any connections that violated this rule after random placement were removed. Si/Al ratios of 4.6 and 10.8 were constructed for the CLI and RHO frameworks, which are hereinafter denoted as CLI-4.6A and RHO-10.8A, respectively. To adequately sample the available aluminum sites within each framework, ten replicates of both zeolites were generated. In these materials, aluminum has an oxidation state of +3, while silicon has +4, leading to a net-negative charge that is balanced by extraframework cations. Equilibration of the extra-framework cation

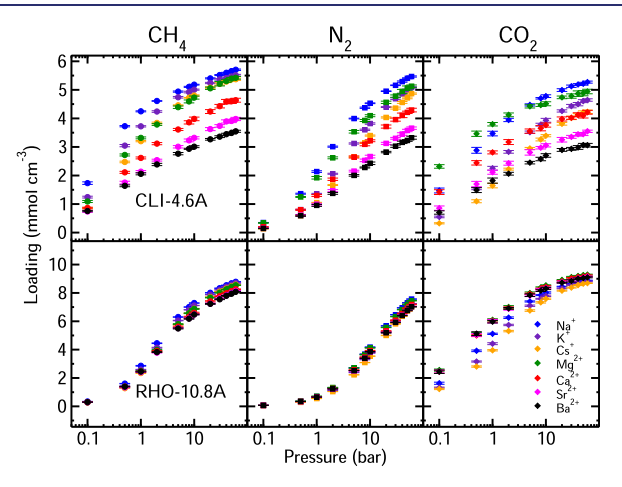


Figure 2. Single-cation adsorption isotherms for CH_4 , N_2 , and CO_2 in CLI-4.6A and RHO-10.8A from 0.1 to 60 bar.

positions was carried out by random generation of starting coordinates, which is different for each replicate, followed by 50,000 cycles of *NVT* (constant particle number, volume, and temperature) MC at 500 K using the MC moves previously described. All cations were observed to rapidly rearrange and occupy sites nearby aluminum.

Nonbonded interactions were represented by the 12-6 LJ, with tail corrections, and Coulomb potential energy functions (eq 1) with cross-terms determined by Lorentz–Berthelot combining rules (eq 2). Long-range charge interactions were calculated by using the Ewald summation technique with a relative precision of 10^{-6} .

$$V_{\text{NB}} = \sum_{i} \sum_{j>i} \left\{ 4\varepsilon_{ij} \left[\left(\frac{\sigma_{ij}}{r_{ij}} \right)^{12} - \left(\frac{\sigma_{ij}}{r_{ij}} \right)^{6} \right] + \frac{q_{i}q_{j}}{r_{ij}} \right\}$$
(1)

$$\sigma_{ij} = \frac{\sigma_i + \sigma_j}{2} \qquad \varepsilon_{ij} = \sqrt{\varepsilon_i \varepsilon_j} \tag{2}$$

LJ and charge parameters for all framework and extraframework atom types were obtained from a study by Dangi et al. in which good agreement between experimental measurements and MC simulation was reported for N₂ and CO₂ adsorption in various cation-exchanged LTL zeolites. In this model, all framework atoms possess charge, but only the zeolite oxygen was considered in the calculation of vdW interactions.

The gases considered in this study were CH₄, N₂, and CO₂, where the TraPPE United Atom³⁰ potential optimized for zeolites,^{31–34} three-site TraPPE Extended Hydrogen,³⁵ and an atomic point charge model developed from ab initio calculations³⁶ were applied to each, respectively. A summary of the compounds and forcefield parameters are shown in Tables 1 and 2, respectively. Chemical potentials for each gas over the specified pressure range were calculated within the RASPA

Table 4. CH₄, N₂, and CO₂ Adsorption at Several Pressures and 298.15 K in Single-Cation Systems of CLI-4.6A^a

		lo	ading (mmol cm ⁻³)			loa	ading (mmol cm ⁻	3)
cation	pressure (bar)	CH ₄	N_2	CO ₂	cation	pressure (bar)	CH ₄	N_2	CO ₂
Na ⁺	0.1	1.73(4)	0.353(3)	1.48(8)	K ⁺	0.1	1.24(3)	0.188(3)	0.55(3)
	0.5	3.73(2)	1.363(18)	2.88(10)		0.5	3.05(4)	0.806(8)	1.54(4)
	1	4.247(18)	2.14(3)	3.47(8)		1	3.72(2)	1.358(18)	2.25(7)
	2	4.610(11)	3.01(2)	3.95(6)		2	4.24(3)	2.061(18)	2.83(5)
	5	4.94(2)	3.996(13)	4.47(4)		5	4.74(3)	3.12(2)	3.52(4)
	8	5.104(19)	4.37(2)	4.70(3)		8	4.92(3)	3.60(2)	3.78(5)
	10	5.182(15)	4.531(14)	4.78(5)		10	5.007(19)	3.82(2)	3.93(7)
	20	5.402(18)	4.953(10)	4.99(5)		20	5.24(2)	4.396(15)	4.26(4)
	30	5.518(18)	5.160(11)	5.13(4)		30	5.37(3)	4.69(3)	4.43(6)
	40	5.597(16)	5.29(2)	5.19(3)		40	5.41(3)	4.86(2)	4.50(6)
	50	5.66(2)	5.405(17)	5.21(5)		50	5.47(3)	5.00(3)	4.60(5)
	60	5.70(2)	5.47(2)	5.27(4)		60	5.51(3)	5.08(3)	4.64(4)
Cs^+	0.1	0.866(18)	0.1341(14)	0.33(2)	Mg^{2+}	0.1	1.09(4)	0.338(11)	2.32(6)
	0.5	2.47(3)	0.595(9)	1.10(5)	-	0.5	2.72(4)	1.248(17)	3.46(9)
	1	3.20(2)	1.051(9)	1.65(8)		1	3.32(3)	1.92(4)	3.80(6)
	2	3.84(3)	1.666(16)	2.22(3)		2	3.79(3)	2.62(3)	4.12(7)
	5	4.458(16)	2.65(2)	2.95(4)		5	4.39(4)	3.53(5)	4.42(6)
	8	4.722(12)	3.14(2)	3.26(5)		8	4.59(5)	3.93(3)	4.47(5)
	10	4.80(2)	3.399(19)	3.39(4)		10	4.73(5)	4.10(3)	4.51(7)
	20	5.08(3)	4.03(2)	3.81(5)		20	5.05(4)	4.56(4)	4.74(5)
	30	5.21(4)	4.36(4)	4.02(6)		30	5.22(8)	4.78(4)	4.78(8)
	40	5.29(4)	4.56(3)	4.12(4)		40	5.31(5)	4.95(7)	4.87(10)
	50	5.37(2)	4.72(3)	4.21(6)		50	5.39(4)	5.06(7)	4.88(9)
	60	5.37(4)	4.87(2)	4.23(6)		60	5.422(5)	5.13(4)	4.94(8)
Ca^{2+}	0.1	0.86(3)	0.200(9)	1.42(8)	Sr^{2+}	0.1	0.74(3)	0.151(4)	0.86(8)
	0.5	2.11(4)	0.80(2)	2.44(8)		0.5	1.75(5)	0.61(3)	1.70(10)
	1	2.61(3)	1.30(3)	2.81(5)		1	2.13(4)	1.00(3)	2.11(7)
	2	3.12(4)	1.87(4)	3.17(9)		2	2.54(3)	1.47(4)	2.43(7)
	5	3.61(4)	2.65(4)	3.55(7)		5	3.01(4)	2.15(3)	2.81(9)
	8	3.86(6)	3.09(5)	3.66(9)		8	3.23(5)	2.53(5)	2.97(4)
	10	3.98(6)	3.22(3)	3.77(7)		10	3.32(4)	2.66(5)	3.06(6)
	20	4.24(7)	3.71(5)	3.98(7)		20	3.63(5)	3.13(4)	3.25(8)
	30	4.43(6)	3.96(5)	4.02(5)		30	3.74(4)	3.30(3)	3.35(5)
	40	4.59(8)	4.11(8)	4.13(7)		40	3.89(6)	3.45(4)	3.44(6)
	50	4.60(8)	4.21(4)	4.10(8)		50	3.91(6)	3.58(4)	3.45(5)
	60	4.64(7)	4.29(6)	4.21(7)		60	3.98(6)	3.66(4)	3.55(4)
Ba ²⁺	0.1	0.76(2)	0.146(8)	0.70(6)					
	0.5	1.64(3)	0.59(2)	1.49(8)					
	1	2.06(4)	0.95(3)	1.82(9)					
	2	2.39(4)	1.37(3)	2.06(5)					
	5	2.77(4)	2.00(3)	2.45(4)					
	8	2.935(19)	2.280(18)	2.58(6)					
	10	3.01(3)	2.43(5)	2.70(6)					
	20	3.27(3)	2.82(3)	2.90(5)					
	30	3.36(3)	3.03(4)	2.93(5)					
	40	3.45(3)	3.16(4)	2.98(7)					
	50	3.49(3)	3.23(3)	3.07(6)					
	60	3.55(4)	3.32(5)	3.06(6)					

 $[^]a\mathrm{The}$ numbers in parentheses represent the 95% confidence level uncertainties in the last digits shown.

software package using the Peng–Robinson equation of state³⁷ and the corresponding critical parameters (Table 3).³⁸

Gas adsorption was calculated using production runs consisting of 100,000 MC cycles after 50,000 MC cycles of equilibration with results averaged over the ten replicate frameworks. Final results were reported at 95% confidence using the Student's *t*-distribution.

3. RESULTS

3.1. Single-Cation Systems. The observed positions, after equilibration, for the cations in CLI and RHO qualitatively agree well with those previously reported. ^{17,22,39} It is important to note, however, that the precise characterization of extraframework cation sites is outside the scope of this study, and the zeolites examined are considered only as representative frameworks to probe the effect of varying cation size and charge.

Table 5. CH₄, N₂, and CO₂ Adsorption at Several Pressures and 298.15 K in Single-Cation Systems of RHO-10.8A^a

	1, 2,	2 1				8	′		
		lo	oading (mmol cm	-3)			lo	oading (mmol cm	-3)
cation	pressure (bar)	CH ₄	N_2	CO ₂	cation	pressure (bar)	CH ₄	N ₂	CO ₂
Na ⁺	0.1	0.345(5)	0.0733(4)	1.63(7)	K ⁺	0.1	0.303(5)	0.0629(4)	1.33(3)
	0.5	1.603(15)	0.3581(19)	3.92(6)		0.5	1.429(14)	0.3074(18)	3.16(4)
	1	2.86(3)	0.695(3)	5.11(4)		1	2.600(13)	0.595(4)	4.42(7)
	2	4.45(2)	1.307(5)	6.25(5)		2	4.14(3)	1.125(5)	5.74(5)
	5	6.300(10)	2.713(13)	7.40(4)		5	6.053(16)	2.386(12)	7.10(5)
	8	7.006(7)	3.684(11)	7.85(3)		8	6.812(13)	3.298(16)	7.59(3)
	10	7.289(10)	4.179(10)	8.03(5)		10	7.116(10)	3.762(12)	7.80(5)
	20	8.010(8)	5.677(11)	8.45(2)		20	7.878(8)	5.248(12)	8.32(3)
	30	8.333(7)	6.463(11)	8.65(2)		30	8.217(5)	6.054(8)	8.57(3)
	40	8.538(7)	6.949(10)	8.77(2)		40	8.436(10)	6.572(18)	8.70(2)
	50	8.681(8)	7.302(9)	8.84(2)		50	8.583(7)	6.958(13)	8.760(19)
	60	8.785(8)	7.568(5)	8.88(2)		60	8.699(10)	7.246(8)	8.81(3)
Cs^+	0.1	0.273(3)	0.0579(5)	1.23(5)	Mg^{2+}	0.1	0.288(4)	0.0763(6)	2.56(8)
	0.5	1.280(8)	0.2833(18)	2.81(5)	-	0.5	1.368(13)	0.370(2)	5.09(12)
	1	2.35(2)	0.551(4)	3.95(5)		1	2.488(18)	0.716(7)	6.10(8)
	2	3.823(19)	1.043(5)	5.31(5)		2	3.98(4)	1.331(10)	7.01(10)
	5	5.77(2)	2.225(7)	6.76(5)		5	5.80(3)	2.708(14)	7.99(7)
	8	6.562(15)	3.090(10)	7.33(5)		8	6.57(3)	3.64(2)	8.38(5)
	10	6.888(14)	3.541(12)	7.59(5)		10	6.87(3)	4.123(17)	8.53(4)
	20	7.705(13)	5.003(16)	8.16(3)		20	7.67(2)	5.565(15)	8.92(3)
	30	8.086(9)	5.816(17)	8.38(3)		30	8.02(3)	6.332(16)	9.11(5)
	40	8.304(7)	6.352(15)	8.55(3)		40	8.250(11)	6.823(15)	9.19(4)
	50	8.461(7)	6.727(13)	8.65(3)		50	8.431(9)	7.19(2)	9.26(3)
	60	8.583(5)	7.030(10)	8.69(2)		60	8.542(19)	7.450(15)	9.29(3)
Ca ²⁺	0.1	0.294(4)	0.0708(7)	2.45(10)	Sr^{2+}	0.1	0.286(3)	0.0688(6)	2.453(10)
	0.5	1.37(2)	0.345(4)	5.00(8)		0.5	1.34(2)	0.335(3)	5.042(10)
	1	2.45(3)	0.673(8)	6.04(10)		1	2.41(2)	0.646(8)	6.00(12)
	2	3.90(3)	1.260(7)	6.94(8)		2	3.79(2)	1.209(8)	6.88(10)
	5	5.62(4)	2.567(10)	7.93(6)		5	5.52(2)	2.500(17)	7.80(6)
	8	6.33(3)	3.476(17)	8.29(4)		8	6.21(3)	3.380(16)	8.22(8)
	10	6.60(4)	3.93(2)	8.42(10)		10	6.48(2)	3.829(12)	8.35(6)
	20	7.41(4)	5.32(2)	8.82(6)		20	7.24(4)	5.21(3)	8.76(7)
	30	7.77(2)	6.08(3)	9.03(5)		30	7.61(2)	5.946(17)	8.87(6)
	40	7.98(3)	6.553(18)	9.13(4)		40	7.82(2)	6.43(2)	9.02(6)
	50	8.13(2)	6.92(2)	9.16(3)		50	8.00(3)	6.77(2)	9.08(6)
	60	8.26(2)	7.18(2)	9.22(5)		60	8.15(2)	7.049(13)	9.15(3)
Ba ²⁺	0.1	0.297(5)	0.0700(6)	2.44(12)					
	0.5	1.39(2)	0.3420(18)	5.13(13)					
	1	2.45(3)	0.654(4)	5.97(9)					
	2	3.83(3)	1.229(8)	6.91(6)					
	5	5.50(4)	2.519(9)	7.84(9)					
	8	6.18(4)	3.395(12)	8.16(6)					
	10	6.48(2)	3.85(2)	8.31(8)					
	20	7.23(3)	5.19(3)	8.72(3)					
	30	7.55(2)	5.925(19)	8.85(8)					
	40	7.80(2)	6.409(12)	9.01(5)					
	50	7.94(3)	6.76(2)	9.051(18)					
	60	8.08(3)	7.023(11)	9.10(4)					
	00	0.00(3)	1.023(11)	9.10(4)					

^aThe numbers in parentheses represent the 95% confidence level uncertainties in the last digits shown.

The adsorption of $\mathrm{CH_4}$, $\mathrm{N_2}$, and $\mathrm{CO_2}$ was calculated over a pressure range of 0.1–60 bar in seven single-cation systems with clear trends in the cation size and charge observed (Figure 2; raw data values are found in Tables 4 and 5). These trends were more pronounced in the CLI framework than the RHO framework, most likely due to their respective 2-dimensional and 3-dimensional pore structures.

In the case of CH₄, whose TraPPE model contains no partial charges, only cation size effects were observed. The magnitude

of adsorption for CH_4 decreased with an increasing cation diameter, σ . Adsorption in the Cs^+ and Mg^{2+} systems was seen to be similar, however. This can be explained by the relative radii and attractive potential of each cation based on the applied interaction parameters, with Mg^{2+} being larger but more attractive and Cs^+ being smaller but less attractive. The same ordering of adsorption was observed for the CLI and RHO frameworks.

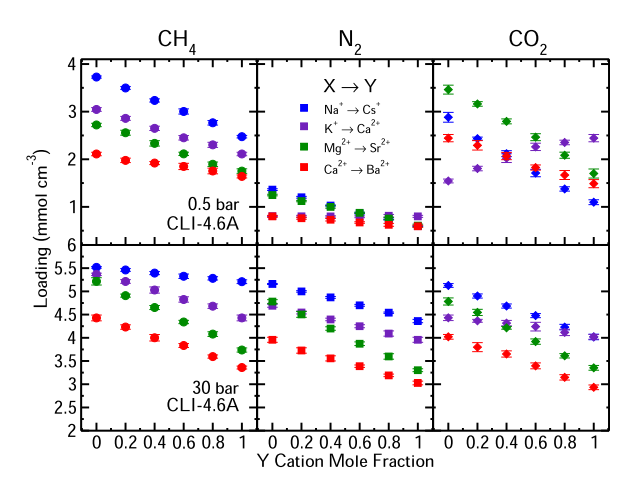
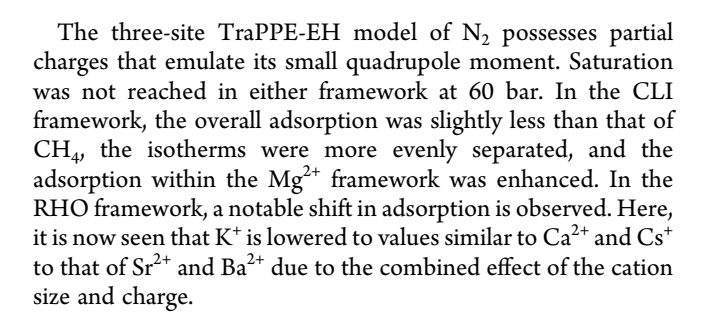


Figure 3. Dependence of adsorption on the cation mole fraction for CH_4 , N_2 , and CO_2 in binary cation CLI-4.6A systems at 0.5 bar (top row) and 30 bar (bottom row).



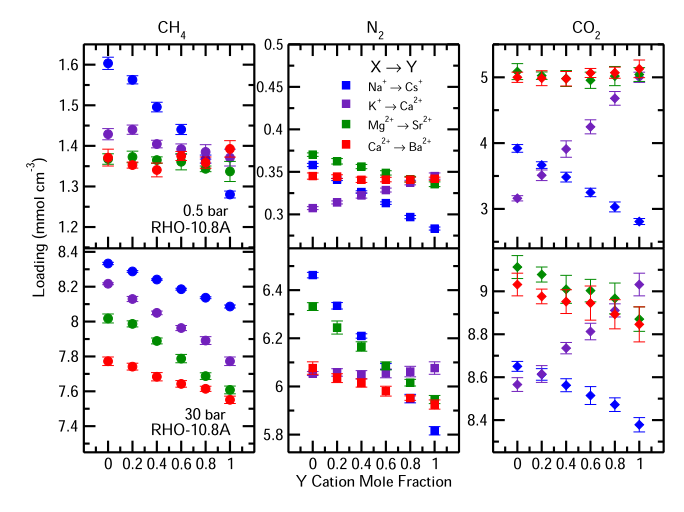


Figure 4. Dependence of adsorption on the cation mole fraction for CH_4 , N_2 , and CO_2 in binary cation RHO-10.8A systems at 0.5 bar (top row) and 30 bar (bottom row).

 CO_2 is larger in size than N_2 and has a larger and more charge interactive quadrupole moment. Loading within the CLI framework showed trends similar to those seen for N_2 adsorption with a notable increase in the Ca^{2+} system relative to Cs^+ . In the RHO framework, CO_2 adsorption was overall higher in the divalent cation systems compared to that in the monovalent systems, resulting from increased charge interactions. Additionally, adsorption was seen to decrease with the increasing cation radius for both the mono- and divalent systems.

Table 6. CH₄, N₂, and CO₂ Adsorption at 0.5 and 30 bar and 298.15 K in Binary Cation Systems of CLI-4.6A^a

	cations	cation mole fraction	load	ling (mmol cm	-3)	cations	cation mole fraction	loa	iding (mmol ci	m^{-3})
pressure (bar)	Х, Ү	X, Y	CH ₄	N_2	CO ₂	X, Y	X, Y	CH_4	N_2	CO_2
0.5	Na+, Cs+	1.0, 0.0	3.73(2)	1.363(18)	2.88(10)	Mg ²⁺ , Sr ²⁺	1.0, 0.0	2.72(4)	1.248(17)	3.46(9)
		0.8, 0.2	3.50(3)	1.202(19)	2.43(3)		0.8, 0.2	2.56(5)	1.122(14)	3.16(5)
		0.6, 0.4	3.24(3)	1.029(12)	2.12(6)		0.6, 0.4	2.33(6)	1.00(3)	2.80(5)
		0.4, 0.6	3.00(5)	0.865(13)	1.71(8)		0.4, 0.6	2.11(3)	0.875(14)	2.46(7)
		0.2, 0.8	2.77(5)	0.735(8)	1.38(5)		0.2, 0.8	1.90(5)	0.75(3)	2.08(6)
		0.0, 1.0	2.47(3)	0.595(9)	1.10(5)		0.0, 1.0	1.75(5)	0.61(3)	1.70(10)
	K+, Ca2+	1.0, 0.0	3.05(4)	0.806(8)	1.54(4)	Ca ²⁺ , Ba ²⁺	1.0, 0.0	2.11(4)	0.80(2)	2.44(8)
		0.8, 0.2	2.86(4)	0.80(2)	1.81(5)		0.8, 0.2	1.98(5)	0.76(2)	2.29(10)
		0.6, 0.4	2.65(4)	0.799(14)	2.02(9)		0.6, 0.4	1.92(3)	0.73(3)	2.07(8)
		0.4, 0.6	2.45(5)	0.792(19)	2.26(8)		0.4, 0.6	1.85(7)	0.672(16)	1.83(5)
		0.2, 0.8	2.30(5)	0.81(3)	2.35(5)		0.2, 0.8	1.75(6)	0.62(3)	1.67(9)
		0.0, 1.0	2.11(4)	0.80(2)	2.44(8)		0.0, 1.0	1.64(3)	0.59(2)	1.49(8)
30	Na+, Cs+	1.0, 0.0	5.518(18)	5.159(11)	5.13(4)	Mg ²⁺ , Sr ²⁺	1.0, 0.0	5.22(8)	4.78(4)	4.78(8)
		0.8, 0.2	5.46(3)	5.000(17)	4.90(5)		0.8, 0.2	4.91(3)	4.50(6)	4.55(7)
		0.6, 0.4	5.39(3)	4.87(2)	4.68(4)		0.6, 0.4	4.65(4)	4.20(4)	4.22(3)
		0.4, 0.6	5.33(5)	4.70(20)	4.48(4)		0.4, 0.6	4.43(4)	3.87(4)	3.92(6)
		0.2, 0.8	5.28(4)	4.542(14)	4.23(6)		0.2, 0.8	4.08(5)	3.60(6)	3.61(5)
		0.0, 1.0	5.21(4)	4.36(4)	4.02(6)		0.0, 1.0	3.74(4)	3.30(3)	3.35(5)
	K+, Ca2+	1.0, 0.0	5.37(3)	4.69(3)	4.43(6)	Ca ²⁺ , Ba ²⁺	1.0, 0.0	4.43(6)	3.40(5)	4.02(5)
		0.8, 0.2	5.21(4)	4.54(3)	4.37(3)		0.8, 0.2	4.23(5)	3.73(6)	3.80(10)
		0.6, 0.4	5.03(7)	4.40(3)	4.32(6)		0.6, 0.4	4.00(7)	3.56(6)	3.65(7)
		0.4, 0.6	4.83(6)	4.25(3)	4.24(9)		0.4, 0.6	3.83(4)	3.39(3)	3.40(6)
		0.2, 0.8	4.68(5)	4.09(6)	4.12(7)		0.2, 0.8	3.60(3)	3.19(3)	3.15(6)
		0.0, 1.0	4.43(6)	3.96(5)	4.02(5)		0.0, 1.0	3.36(3)	3.03(4)	2.93(5)

^aThe numbers in parentheses represent the 95% confidence level uncertainties in the last digits shown.

Table 7. Randomly Generated Cation Mole Fractions for CLI-4.6A and RHO-10.8A

	CLI-4.6A	RHO-10.8A
cation	cation	cation
	mole fraction	mole fraction
Na ⁺	0.130	0.118
K ⁺	0.113	0.109
Cs ⁺	0.226	0.209
Cs^+ Mg^{2+} Ca^{2+}	0.174	0.182
Ca ²⁺	0.130	0.145
Sr ²⁺	0.061	0.055
Ba ²⁺	0.165	0.182

3.2. Two-Cation Systems. To determine how cation effects combine to influence adsorption, several two-cation systems were simulated at 0.5 and 30 bar (Figures 3 and 4; raw data values are found in Tables 6 and 8). This analysis serves to fill in the gaps that separate the single-cation isotherms. The results are represented as independent single-cation systems gradually becoming a different single-cation system through 0.2 mol fraction increments of the intermediate two-cation mixtures ($X \rightarrow Y$). The x-axis in Figures 3 and 4 gives the increasing mole fraction of the "Y" cation, where zero and one are the single-cation adsorptions of the "X" and "Y" cations, respectively, from Figure 2. Mixtures containing cations of similar charge but differing size and differing charge were examined.

The approximate linearity of every system tested seems to suggest that the adsorption effect that each cation contributes is approximately additive at both low and high pressure. The

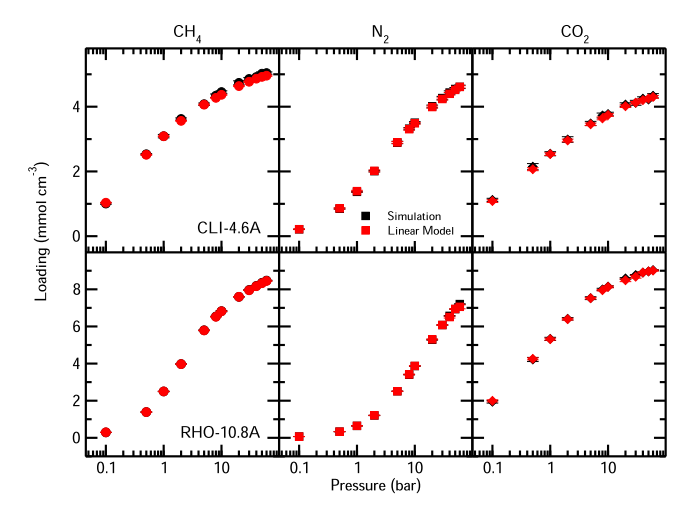


Figure 5. Comparison of simulated (black) and predicted (red) adsorption for CH_4 , N_2 , and CO_2 random CLI-4.6A (top row) and RHO-10.8A (bottom row) systems.

slopes of the data shown also agree with the direction that the single-cation isotherms would suggest between the cation pair.

4. LINEAR MODEL

If one assumes that the adsorption effect of the cations in higher order mixtures remains additive, then the single-cation isotherms would contain all the information needed to predict the results of simulating those mixtures. Equations 3 and 4 show how the adsorption in such mixtures and its variance can be calculated by summing together the adsorption in single-cation

Table 8. CH₄, N₂, and CO₂ Adsorption 0.5 and 30 bar and 298.15 K in Binary Cation Systems of RHO-10.8A^a

	cations	cation mole fraction	load	ding (mmol cm	-3)	cations	cation mole fraction	loa	ding (mmol cm	-3)
pressure (bar)	Х, Ү	X, Y	CH ₄	N_2	CO ₂	Х, Ү	X, Y	CH ₄	N_2	CO ₂
0.5	Na+, Cs+	1.0, 0.0	1.603(15)	0.3581(19)	3.92(6)	Mg ²⁺ , Sr ²⁺	1.0, 0.0	1.367(13)	0.370(2)	5.09(12)
		0.8, 0.2	1.563(10)	0.3410(12)	3.67(5)		0.8, 0.2	1.373(14)	0.362(3)	5.02(6)
		0.6, 0.4	1.496(12)	0.3263(15)	3.48(7)		0.6, 0.4	1.365(8)	0.356(3)	4.98(12)
		0.4, 0.6	1.440(13)	0.3132(15)	3.25(6)		0.4, 0.6	1.36(2)	0.349(3)	4.95(12)
		0.2, 0.8	1.367(10)	0.2968(19)	3.03(8)		0.2, 0.8	1.343(7)	0.341(3)	5.02(15)
		0.0, 1.0	1.280(8)	0.2833(18)	2.81(5)		0.0, 1.0	1.34(2)	0.335(3)	5.04(10)
	K+, Ca2+	1.0, 0.0	1.429(14)	0.3074(18)	3.16(4)	Ca ²⁺ , Ba ²⁺	1.0, 0.0	1.37(2)	0.345(4)	5.00(8)
		0.8, 0.2	1.440(11)	0.3140(18)	3.51(8)		0.8, 0.2	1.35(7)	0.344(2)	4.99(11)
		0.6, 0.4	1.404(9)	0.322(3)	3.91(12)		0.6, 0.4	1.341(17)	0.341(3)	4.98(11)
		0.4, 0.6	1.392(13)	0.329(2)	4.25(11)		0.4, 0.6	1.375(11)	0.341(3)	5.07(7)
		0.2, 0.8	1.385(18)	0.337(3)	4.68(10)		0.2, 0.8	1.359(14)	0.341(3)	5.07(8)
		0.0, 1.0	1.37(2)	0.345(4)	5.00(8)		0.0, 1.0	1.40(2)	0.3420(18)	5.13(13)
30	Na+, Cs+	1.0, 0.0	8.333(7)	6.463(11)	8.65(2)	Mg ²⁺ , Sr ²⁺	1.0, 0.0	8.02(3)	6.332(16)	9.11(5)
		0.8, 0.2	8.287(5)	6.335(13)	8.61(3)		0.8, 0.2	7.987(17)	6.24(3)	9.08(4)
		0.6, 0.4	8.241(4)	6.210(9)	8.56(3)		0.6, 0.4	7.889(17)	6.17(2)	9.01(7)
		0.4, 0.6	8.185(5)	6.083(12)	8.51(4)		0.4, 0.6	7.79(2)	6.085(16)	9.00(5)
		0.2, 0.8	8.137(5)	5.950(18)	8.47(3)		0.2, 0.8	7.687(19)	6.016(14)	8.97(7)
		0.0, 1.0	8.086(9)	5.816(17)	8.38(3)		0.0, 1.0	7.61(2)	5.946(17)	8.87(6)
	K+, Ca2+	1.0, 0.0	8.217(5)	6.053(8)	8.57(3)	Ca ²⁺ , Ba ²⁺	1.0, 0.0	7.77(2)	6.08(3)	9.03(5)
		0.8, 0.2	8.130(15)	6.058(16)	8.61(4)		0.8, 0.2	7.74(2)	6.035(18)	8.98(3)
		0.6, 0.4	8.050(10)	6.049(17)	8.74(3)		0.6, 0.4	7.68(2)	6.014(17)	8.95(6)
		0.4, 0.6	7.963(15)	6.054(18)	8.81(4)		0.4, 0.6	7.643(19)	5.98(2)	8.95(8)
		0.2, 0.8	7.89(2)	6.06(2)	8.91(3)		0.2, 0.8	7.614(15)	5.952(9)	8.89(7)
		0.0, 1.0	7.77(2)	6.08(3)	9.03(5)		0.0, 1.0	7.55(2)	5.925(19)	8.85(8)

^aThe numbers in parentheses represent the 95% confidence level uncertainties in the last digits shown.

Table 9. CH_4 , N_2 , and CO_2 Adsorption at Several Pressures and 298.15 K in Random Cation Compositions of CLI-4.6A and RHO-10.8A^a

		simulation	linear model	simulation	linear model
adsorbate	pressure (bar)	CLI-4.6A	CLI-4.6A	RHO-10.8A	RHO-10.8A
		loading (mmol cm^{-3})	loading (mmol cm^{-3})	loading (mmol cm^{-3})	loading (mmol cm ⁻
CH ₄	0.1	1.01(2)	1.034(12)	0.292(3)	0.2957(16)
	0.5	2.53(2)	2.516(13)	1.387(10)	1.387(6)
	1	3.09(5)	3.087(11)	2.500(13)	2.498(10)
	2	3.62(3)	3.563(13)	3.97(2)	3.970(12)
	5	4.08(4)	4.063(13)	5.79(2)	5.785(11)
	8	4.34(5)	4.274(13)	6.535(14)	6.521(10)
	10	4.45(4)	4.368(15)	6.83(3)	6.818(10)
	20	4.74(6)	4.637(15)	7.595(13)	7.600(10)
	30	4.86(4)	4.77(2)	7.966(19)	7.948(7)
	40	4.92(5)	4.866(17)	8.183(13)	8.170(7)
	50	5.02(6)	4.921(16)	8.352(13)	8.329(6)
	60	5.04(4)	4.958(17)	8.470(19)	8.450(7)
N_2	0.1	0.213(4)	0.216(13)	0.0681(6)	0.068(4)
	0.5	0.851(18)	0.86(2)	0.332(2)	0.333(9)
	1	1.370(15)	1.39(3)	0.643(4)	0.644(13)
	2	2.01(2)	2.02(3)	1.203(9)	1.210(12)
	5	2.89(4)	2.90(3)	2.508(8)	2.506(15)
	8	3.32(3)	3.31(3)	3.404(10)	3.41(2)
	10	3.51(3)	3.49(3)	3.87(2)	3.87(2)
	20	4.01(4)	3.99(3)	5.28(2)	5.30(2)
	30	4.27(5)	4.24(3)	6.08(2)	6.08(2)
	40	4.44(5)	4.40(4)	6.570(18)	6.50(5)
	50	4.55(4)	4.52(3)	6.934(10)	6.94(2)
	60	4.61(5)	4.61(4)	7.207(9)	7.06(11)
CO_2	0.1	1.12(5)	1.09(4)	1.94(7)	1.99(6)
	0.5	2.15(9)	2.07(5)	4.220(11)	4.25(5)
	1	2.55(6)	2.54(4)	5.33(9)	5.31(5)
	2	2.99(9)	2.96(4)	6.41(7)	6.39(5)
	5	3.48(7)	3.46(4)	7.52(8)	7.52(4)
	8	3.73(8)	3.64(4)	7.99(6)	7.95(4)
	10	3.77(6)	3.74(4)	8.15(4)	8.13(5)
	20	4.07(6)	4.01(4)	8.59(4)	8.49(7)
	30	4.12(8)	4.12(4)	8.77(3)	8.68(8)
	40	4.25(6)	4.20(4)	8.90(4)	8.90(3)
	50	4.22(3)	4.25(4)	8.97(3)	8.97(3)
	60	4.34(7)	4.30(4)	9.04(2)	9.01(3)

^aThe numbers in parentheses represent the 95% confidence level uncertainties in the last digits shown.

systems, l_i , multiplied by the mole fractions present in the mixture, x_i .

$$L = \sum_{i} x_i l_i \tag{3}$$

$$\delta L^2 = \sum_i (x_i \delta l_i)^2 \tag{4}$$

To test this approach, random cation mixtures made up of all seven cations explored in this study were created for CLI-4.6A and RHO-10.8A. This was done by normalizing a set of seven randomly generated numbers to ensure that the total mole fraction for the cation mixture was added to one (Table 7).

These systems were built and equilibrated with the procedure detailed previously, and isotherms from 0.1 to 60 bar were calculated (Figure 5, black; raw data values given in Table 9). The single-cation adsorption values were then used in eqs 3 and 4 alongside the randomly generated mole fractions to predict the

adsorption and its uncertainty over the same pressure range (Figure 5, red; raw data values are found in Table 9).

The final isotherms are in excellent agreement, suggesting that for the zeolites considered in this study, the adsorption effects of cations up to a seven-cation mixture can be well approximated as additive in the absence of a significant structural change. Note that the application of this linear model does not necessarily require evaluation of the single-cation adsorption data. For a system with n cations, it is sufficient to have adsorption data from n linearly independent sets of cation compositions for a given zeolite to calculate the linear coefficients in eq 3.

5. CONCLUSIONS

The cation dependence of CH_4 , N_2 , and CO_2 gas adsorption was explored through single-, two-, and seven-cation systems within CLI-4.6A and RHO-10.8A frameworks. Clear trends relating to the size and charge of each cation relative to the adsorbate were observed in both the single- and two-cation systems. The mole fraction dependence of the two-cation adsorption was seen to be

linear to a good approximation, suggesting that the combined effect on adsorption from each cation is approximately additive. This linearity suggests that the adsorption of gases in natural zeolites with mixed cation types can reasonably be approximated from measurements of single-cation adsorption. This was confirmed by calculating the gas adsorption within randomly generated seven-cation zeolites both through direct simulation and by application of a linear model based on single-cation simulations. Excellent agreement was seen between the simulated and predicted results.

Given the limitations and approximations in this work (a limited number of framework structures and Si/Al ratios, as well as the use of model potentials and idealized structures), additional simulation studies (e.g., on a wider range of Si/Al values and zeolite topologies) as well as experimental validation would be beneficial. Also, as gas separations are combined thermodynamic and kinetic processes, the cation dependence of gas diffusion would be a logical next step.

ASSOCIATED CONTENT

Supporting Information

The Supporting Information is available free of charge at https://pubs.acs.org/doi/10.1021/acs.jced.3c00727.

Simulation details of RHO_5_3Al and CLI_276AL (ZIP)

AUTHOR INFORMATION

Corresponding Author

Brian B. Laird — Department of Chemistry, University of Kansas, Lawrence, Kansas 66045, United States; Wonderful Institute for Sustainable Engineering, University of Kansas, Lawrence, Kansas 66045, United States; Occid.org/0000-0003-1859-732X; Email: blaird@ku.edu

Author

Micah L. Welsch — Department of Chemistry, University of Kansas, Lawrence, Kansas 66045, United States; Wonderful Institute for Sustainable Engineering, University of Kansas, Lawrence, Kansas 66045, United States

Complete contact information is available at: https://pubs.acs.org/10.1021/acs.jced.3c00727

Notes

The authors declare no competing financial interest.

ACKNOWLEDGMENTS

The authors would like to thank Prof. Mark B. Shiflett and Dr. David R. Corbin from the Wonderful Institute for Sustainable Engineering at the University of Kansas for their financial and technical support on this project.

REFERENCES

- (1) Li, H.; Wang, K.; Sun, Y.; Lollar, C. T.; Li, J.; Zhou, H. C. Recent advances in gas storage and separation using metal—organic frameworks. *Mater. Today* **2018**, *21*, 108–121.
- (2) Rufford, T.; Smart, S.; Watson, G.; Graham, B.; Boxall, J.; Diniz da Costa, J.; May, E. The removal of CO₂ and N₂ from natural gas: A review of conventional and emerging process technologies. *J. Pet. Sci. Eng.* **2012**, *94*–*95*, 123–154.
- (3) Kammerer, S.; Borho, I.; Jung, J.; Schmidt, M. Review: CO₂ capturing methods of the last two decades. *Int. J. Environ. Sci. Technol.* **2023**, 20, 8087–8104.

- (4) Ojha, D. K.; Kale, M. J.; McCormick, A. V.; Reese, M.; Malmali, M.; Dauenhauer, P.; Cussler, E. L. Integrated ammonia synthesis and separation. *ACS Sustain. Chem. Eng.* **2019**, *7*, 18785–18792.
- (5) Ray, K. G.; Olmsted, D. L.; Burton, J. M.; Houndonougbo, Y.; Laird, B. B.; Asta, M. Gas membrane selectivity enabled by zeolitic imidazolate framework electrostatics. *Chem. Mater.* **2014**, *26*, 3976–3085
- (6) Chang, M.; Yan, T.; Wei, Y.; Wang, J. X.; Liu, D.; Chen, J. F. Enhancing CH₄ Capture from Coalbed Methane through Tuning van der Waals Affinity within Isoreticular Al-Based Metal-Organic Frameworks. ACS Appl. Mater. Interfaces 2022, 14, 25374–25384.
- (7) DeSantis, D.; Mason, J. A.; James, B. D.; Houchins, C.; Long, J. R.; Veenstra, M. Techno-economic analysis of metal-organic frameworks for hydrogen and natural gas storage. *Energy Fuels* **2017**, *31*, 2024–2032.
- (8) He, Q.; Zhan, F.; Wang, H.; Xu, W.; Wang, H.; Chen, L. Recent progress of industrial preparation of metal—organic frameworks: synthesis strategies and outlook. *Mater. Today Sustain.* **2022**, 17, 100104
- (9) Pérez-Botella, E.; Valencia, S.; Rey, F. Zeolites in adsorption processes: State of the art and future prospects. *Chem. Rev.* **2022**, *122*, 17647–17695.
- (10) Ackley, M. W.; Rege, S. U.; Saxena, H. Application of natural zeolites in the purification and separation of gases. *Microporous Mesoporous Mater.* **2003**, *61*, 25–42.
- (11) Boer, D. G.; Langerak, J.; Pescarmona, P. P. Zeolites as Selective Adsorbents for CO₂ Separation. ACS Appl. Energy Mater. 2023, 6, 2634–2656.
- (12) Ackley, M. W.; Giese, R. F.; Yang, R. T. Clinoptilolite: Untapped potential for kinetics gas separations. *Zeolites* **1992**, *12*, 780–788.
- (13) Abdelrasoul, A.; Zhang, H.; Cheng, C. H.; Doan, H. Applications of molecular simulations for separation and adsorption in zeolites. *Microporous Mesoporous Mater.* **2017**, 242, 294–348.
- (14) Smit, B.; Maesen, T. L. Molecular simulations of zeolites: Adsorption, diffusion, and shape selectivity. *Chem. Rev.* **2008**, *108*, 4125–4184.
- (15) Dib, E.; Clatworthy, E. B.; Paecklar, A. A.; Grand, J.; Barrier, N.; Mintova, S. Role of Al distribution in CO₂ adsorption capacity in RHO zeolites. *J. Phys. Chem. C* **2023**, *127*, 3–10.
- (16) Liang, D.; Hu, Y.; Bao, Q.; Zhang, J.; Sun, P.; Feng, J.; Xu, M.; Zhang, H. Study of RHO zeolite with different cations for CO_2/CO separation in pressure swing adsorption. *Micro Nano Lett.* **2021**, *16*, 319–326.
- (17) Lozinska, M. M.; Mangano, E.; Mowat, J. P.; Shepherd, A. M.; Howe, R. F.; Thompson, S. P.; Parker, J. E.; Brandani, S.; Wright, P. A. Understanding carbon dioxide adsorption on univalent cation forms of the flexible zeolite RHO at conditions relevant to carbon capture from flue gases. *J. Am. Chem. Soc.* **2012**, *134*, 17628–17642.
- (18) Ridha, F. N.; Yang, Y.; Webley, P. A. Adsorption characteristics of a fully exchanged potassium chabazite zeolite prepared from decomposition of zeolite Y. *Microporous Mesoporous Mater.* **2009**, 117, 497–507.
- (19) Beerdsen, E.; Dubbeldam, D.; Smit, B.; Vlugt, T. J.; Calero, S. Simulating the effect of nonframework cations on the adsorption of alkanes in MFI-type zeolites. *J. Phys. Chem. B* **2003**, *107*, 12088–12096.
- (20) Dangi, G. P.; Munusamy, K.; Somani, R. S.; Bajaj, H. C. Adsorption selectivity of CO₂ over N₂ by cation exchanged zeolite L: Experimental and simulation studies. *Indian J. Chem., Sect. A: Inorg., Phys., Theor. Anal.* **2012**, *51A*, 1238–1251.
- (21) Maurin, G.; Llewellyn, P.; Poyet, T.; Kuchta, B. Influence of extra-framework cations on the adsorption properties of X-faujasite systems: Microcalorimetry and molecular simulations. *J. Phys. Chem. B* **2005**, *109*, 125–129.
- (22) Kennedy, D. A.; Tezel, F. H. Cation exchange modification of clinoptilolite Screening analysis for potential equilibrium and kinetic adsorption separations involving methane, nitrogen, and carbon dioxide. *Microporous Mesoporous Mater.* **2018**, 262, 235–250.

- (23) Palomino, M.; Corma, A.; Jordá, J. L.; Rey, F.; Valencia, S. Zeolite RHO: A highly selective adsorbent for CO₂/CH₄ separation induced by a structural phase modification. *Chem. Commun.* **2012**, *48*, 215–217.
- (24) Shi, W.; Maginn, E. J. Continuous fractional component Monte Carlo: An adaptive biasing method for open system atomistic simulations. *J. Chem. Theory Comput.* **2007**, *3*, 1451–1463.
- (25) Dubbeldam, D.; Calero, S.; Ellis, D. E.; Snurr, R. Q. RASPA: Molecular simulation software for adsorption and diffusion in flexible nanoporous materials. *Mol. Simul.* **2016**, *42*, 81–101.
- (26) Baerlocher, C.; McCusker, L. Database of Zeolite Structures. http://www.iza-structure.org/databases/ (accessed May 19, 2019).
- (27) Stukowski, A. Visualization and analysis of atomistic simulation data with OVITO-the Open Visualization Tool. *Modell. Simul. Mater. Sci. Eng.* **2010**, *18*, 015012.
- (28) Pinar, A. B.; Rzepka, P.; Knorpp, A. J.; McCusker, L. B.; Baerlocher, C.; Huthwelker, T.; van Bokhoven, J. A. Pinpointing and quantifying the aluminum distribution in zeolite catalysts using anomalous scattering at the Al absorption edge. *J. Am. Chem. Soc.* **2021**, *143*, 17926–17930.
- (29) Fletcher, R. E.; Ling, S.; Slater, B. Violations of Löwenstein's rule in zeolites. *Chem. Sci.* **2017**, *8*, 7483–7491.
- (30) Martin, M.; Siepmann, J. Transferable potentials for phase equilibria. 1. United-atom description of n-alkanes. *J. Phys. Chem. B* **1998**, *102*, 2569–2577.
- (31) Dubbeldam, D.; Calero, S.; Vlugt, T. J.; Krishna, R.; Maesen, T. L.; Smit, B. United atom force field for alkanes in nanoporous materials. *J. Phys. Chem. B* **2004**, *108*, 12301–12313.
- (32) García-Pérez, E.; Parra, J. B.; Ania, C. O.; García-Sánchez, A.; Van Baten, J. M.; Krishna, R.; Dubbeldam, D.; Calero, S. A computational study of CO₂, N₂, and CH₄ adsorption in zeolites. *Adsorption* **2007**, *13*, 469–476.
- (33) Krishna, R.; van Baten, J. M. In silico screening of zeolite membranes for CO₂ capture. *J. Membr. Sci.* **2010**, *360*, 323–333.
- (34) Liu, B.; Smit, B. Comparative molecular simulation study of CO_2/N_2 and CH_4/N_2 separation in zeolites and metal-organic frameworks. *Langmuir* **2009**, *25*, 5918–5926.
- (35) Potoff, J.; Siepmann, J. Vapor-liquid equilibria of mixtures containing alkanes, carbon dioxide and nitrogen. *AIChE J.* **2001**, 47, 1676–1682.
- (36) Maurin, G.; Llewellyn, P. L.; Bell, R. G. Adsorption mechanism of carbon dioxide in faujasites: Grand canonical Monte Carlo simulations and microcalorimetry measurements. *J. Phys. Chem. B* **2005**, *109*, 16084–16091.
- (37) Peng, D.-Y.; Robinson, D. B. A New Two-Constant Equation of State. *Int. J. Heat Mass Transfer* **1973**, 19, 1469.
- (38) Reid, R. C.; Prausnitz, J. M.; Poling, B. E. The Properties of Gases and Liquids, 4th ed.; McGraw-Hill: New York, 1987.
- (39) Uzunova, E. L.; Mikosch, H. Cation site preference in zeolite clinoptilolite: A density functional study. *Microporous Mesoporous Mater.* **2013**, 177, 113–119.